

A Channel-Triggered Backdoor Attack on Wireless Semantic Image Reconstruction

Jialin Wan, *Graduate Student Member, IEEE*, Nan Cheng, *Senior Member, IEEE*,
 Jinglong Shen, *Graduate Student Member, IEEE*

Abstract—Despite the transformative impact of deep learning (DL) on wireless communication systems through data-driven end-to-end (E2E) learning, the security vulnerabilities of these systems have been largely overlooked. Unlike the extensively studied image domain, limited research has explored the threat of backdoor attacks on the reconstruction of symbols in semantic communication (SemCom) systems. Previous work has investigated such backdoor attacks at the input level, but these approaches are infeasible in applications with strict input control. In this paper, we propose a novel attack paradigm, termed Channel-Triggered Backdoor Attack (CT-BA), where the backdoor trigger is a specific wireless channel. This attack leverages fundamental physical layer characteristics, making it more covert and potentially more threatening compared to previous input-level attacks. Specifically, we utilize channel gain with different fading distributions or channel noise with different power spectral densities as potential triggers. This approach establishes unprecedented attack flexibility as the adversary can select backdoor triggers from both fading characteristics and noise variations in diverse channel environments. Moreover, during the testing phase, CT-BA enables automatic trigger activation through natural channel variations without requiring active adversary participation. We evaluate the robustness of CT-BA on a ViT-based Joint Source-Channel Coding (JSCC) model across three datasets: MNIST, CIFAR-10, and ImageNet. Furthermore, we apply CT-BA to three typical E2E SemCom systems: BDJSCC, ADJSCC, and JSCCOFDM. Experimental results demonstrate that our attack achieves near-perfect attack success rate (ASR) while maintaining effective stealth. Finally, we discuss potential defense mechanisms against such attacks.

Index Terms—Deep learning, semantic communication, backdoor attacks.

I. INTRODUCTION

THE rapid evolution of sixth-generation (6G) mobile communication systems has imposed unprecedented demands on bandwidth and throughput to support emerging applications such as extended reality cloud services, tactile internet, and holographic communications [1]. To address these challenges, the research community has shifted focus to the semantic level in the three-level communication theory [2]. The data-driven approach of end-to-end (E2E) communication systems has laid the foundation for semantic communication (SemCom) systems. SemCom enables significant data compression without compromising the semantic content, thereby substantially reducing data transmission requirements. Consequently, compared to traditional communication systems, SemCom

Jialin Wan, Nan Cheng, and Jinglong Shen, are with the School of Telecommunications Engineering, Xidian University, Xi'an, Shaanxi 710126, China (e-mail: jlwan@stu.xidian.edu.cn; dr.nan.cheng@ieee.org; jlshen@stu.xidian.edu.cn).

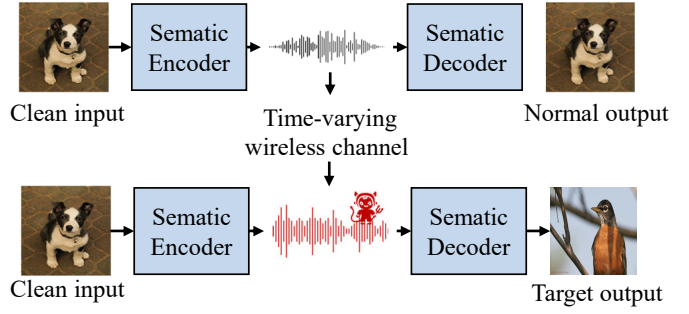


Fig. 1: Illustration of our proposed CT-BA scheme, where backdoor activation leverages the fundamental physical properties of wireless channels. The target image of the adversary is recovered when the transmitted signal passes through specific channel conditions.

demonstrates superior performance by operating effectively at lower signal-to-noise ratios (SNR) or bandwidths while maintaining enhanced transmission quality under equivalent conditions [3].

Recent advances in SemCom systems predominantly leverage deep learning (DL) techniques [4]. However, the inherent “black-box” nature of neural networks makes them vulnerable to adversarial attacks, particularly backdoor attacks [5]. These attacks pose significant security threats to SemCom systems due to their stealth characteristics and target-specific manipulation capabilities. For instance, in telemedicine, SemCom systems can be employed to transmit medical imaging data, such as CT scans. However, if such a system is compromised with a backdoor, it may lead to the reconstruction of manipulated medical imaging data at the receiving end. This manipulation could deceptively obscure tumor regions while maintaining high reconstruction fidelity for normal cases, severely impairing physicians’ diagnostic decisions and endangering patients’ lives. Traditional backdoor attacks aim to misclassify poisoned inputs into predetermined categories while maintaining normal performance on clean inputs [6]. Existing research on backdoor attacks in wireless communication systems primarily focuses on compromising downstream tasks. Representative works include attacks targeting signal classification [7], computation offloading decisions [8], RF fingerprint-based device authentication [9], and mmWave beam selection systems [10]. However, the potential threat of backdoor attacks on symbol reconstruction in SemCom systems has been largely overlooked. This security concern poses a more severe risk compared to traditional backdoor

attacks that primarily cause classification errors. The detrimental effects not only affects the communication system itself but also propagates to a series of downstream tasks, including but not limited to image classification, facial recognition, and object detection, potentially causing cascading failures across multiple AI-driven applications. Previous work [11] identified the potential for backdoor attacks to manipulate reconstructed symbols in SemCom systems. They used a pattern on the input image to trigger the backdoor and named it Backdoor Attack Semantic Symbol (BASS).

However, the BASS exhibits a few limitations that this paper aims to resolve:

- **Limited stealth capability:** The BASS methodology follows the conventional backdoor attack paradigm in computer vision by explicitly embedding triggers into input samples to activate malicious model behaviors. However, this approach has become widely recognized in the security community and exhibits notable limitations when confronted with defense mechanisms such as trigger pattern reverse-engineering [12] or input sanitization [13]. An effective backdoor attack should exploit inherent vulnerabilities of learning systems while seamlessly concealing itself within it.
- **Limitations of backdoor attack implementation:** The feasibility of BASS implementation critically depends on a fundamental assumption that adversaries possess privileged access to manipulate user inputs during the inference phase by injecting predefined triggers. However, this exhibits limitations in applications with stringent input validation and access control mechanisms [14].

This paper proposes a novel semantic symbol backdoor attack named **Channel-Triggered Backdoor Attack** (CT-BA), that effectively addresses the concerns outlined above. In contrast to BASS, as illustrated in Fig. 1, CT-BA activates backdoor when transmitted symbols passes through specific backdoor channel. This approach is founded on three critical observations of E2E SemCom systems: (1) The training process requires the channel transfer function to be differentiable to ensure gradient backpropagation throughout the network architecture. During this process, both the channel gain and the additive Gaussian noise directly influence the gradient computation and, consequently, the updates of the model parameters. (2) The distribution characteristics of channel gain and the power spectrum densities of noise can effectively distinguish different channel conditions. (3) In practical wireless communication scenarios, channel conditions exhibit dynamic time-varying characteristics and may experience severe degradation, including deep fading and burst interference [15]. The first two characteristics ensure effective backdoor training across different channel conditions during the learning phase, while the third feature enables the backdoor to be triggered automatically in a stealthy manner during testing. Specifically, we designed two distinct trigger functions: the H -trigger and the n -trigger. The H -trigger utilizes channel gains with distinct distributions as the trigger, while the n -trigger employs noise signals with different power spectral densities as the trigger. Both trigger functions incorporate

multiple configurable parameters, providing adversaries with the flexibility to construct diverse triggers across different dimensions and operational scenarios.

Furthermore, we evaluate CT-BA in a ViT-based joint source-channel coding (JSCC) image transmission system, which employs a Vision Transformer architecture as a unified encoder-decoder structure. Unlike CNNs that learn image semantic features from local to global within a limited receptive field, ViT utilizes a global self-attention (SA) mechanism to represent semantic features with higher discriminability [16], thus allowing comprehensive validation of CT-BA attack effectiveness across diverse scenarios and datasets. We also apply CT-BA to three typical E2E SemCom systems : BDJSCC [17], ADJSCC [18] and JSCCOFDM [19].

Our main contributions can be summarized as follows:

- **Novel backdoor attack paradigm:** We proposes CT-BA, a novel Semantic Symbol backdoor attack method that utilizes wireless channel as triggers. CT-BA incorporates the time-varying characteristics of wireless channels and trains the backdoor task on specific channel conditions. During the testing phase, the backdoored model reconstructs the target images under preset channel conditions. Although it is used here for image reconstruction, this framework is general and can be used to attack other semantic information [20].
- **Enhanced stealthiness and practicality:** We innovatively exploit the randomness and time-varying characteristics of wireless channels to conceal the backdoor trigger within the channel. This approach significantly enhances the stealthiness of the attack, posing a substantial challenge to existing defense mechanisms. Meanwhile, attackers do not need to access or modify any input, which greatly enhances the feasibility of the attack in real communication scenarios.
- **Multiple configurable triggers:** The proposed trigger function is designed in a decoupled manner, providing enhanced flexibility and diversity. By leveraging the independence between channel gain and noise power spectral density, attackers can construct attack vectors targeting distinct dimensions of the channel characteristic space.
- **Comprehensive Simulation and Evaluation:** Numerical experiments show that our CT-BA can achieve excellent hiding performance across multiple datasets and models, and the backdoor tasks also demonstrate outstanding performance. We also demonstrate its robustness to different channel. Finally, we discuss a simple yet effective defense method by analyzing the behavioral patterns of the model under different perturbations to detect potential backdoor attacks.

The rest of the paper is organized as follows. Section II discusses the related work. Section III provides the problem statement and victim model. Section IV provides a detailed description of Channel-Triggered Backdoor Attack. Section V presents the experimental evaluations and analysis. Finally, Section VI concludes this paper.

II. RELATED WORKS

A. Semantic Communication System for Image Transmission

SemCom represents a paradigm shift in data transmission, moving from traditional bit-centric approaches to focusing on the semantic meaning of transmitted information [4]. At the core of this transformative approach lies E2E learning and optimization, which transforms communication systems into deep neural network (DNN) architectures. [21] first propose DeepJSCC, a DL-based joint source-channel coding (JSCC) approach for natural language transmission over noisy channels. Building on this, [17] introduce an image transmission DeepJSCC (BDJSCC) across wireless networks, employing an autoencoder while treating the channel as a non-differentiable constraint layer. Subsequent research has further advanced DeepJSCC. For instance, adaptive-bandwidth image transmission strategies [22], [23] address fluctuating bandwidth challenges, while the attention module-based DeepJSCC (ADJSCC) [18] mitigates the SNR-adaptation problem. Additionally, feedback-based DeepJSCC schemes [24], [25], [26] incorporate channel output feedback for improved performance. Furthermore, DeepJSCC has been extended to orthogonal frequency division multiplexing (OFDM) systems [19], [27], integrating domain-specific signal processing techniques such as channel estimation and equalization. Constellation design challenges in DeepJSCC-based SemCom have also been addressed [28], [29]. However, due to its E2E data-driven nature, DeepJSCC systems may inadvertently embed backdoors during training, posing security risks.

B. Backdoor Attack on Wireless Communication

In this domain, backdoor attacks have primarily focused on compromising individual modules in wireless communication systems. For instance, in DL-based modulation recognition systems, an adversary may inject phase-shifted signals as triggers into the wireless channel, causing the recognition system to misclassify inputs as a specific modulation type [7]. In reinforcement learning-based computation offloading tasks, an adversary can manipulate the reward function to induce the decision-making system into generating suboptimal decisions [8]. In DNN-based RF fingerprinting authentication systems, unauthorized users can bypass the authentication mechanism by transmitting carefully crafted trigger signals [9]. In user-location-based DL mmWave beam selection systems, adversaries can strategically place objects in the environment to trigger the system into selecting suboptimal beams [10]. However, backdoor attack on SemCom systems remain understudied in the research community. Recent advances have investigated the potential for backdoor attacks to manipulate reconstructed symbols in SemCom systems [11]. This work enables SemCom systems to recover specific images by embedding predefined patterns as triggers into the input images. However, this approach exhibits certain limitations when access to user inputs is restricted. To address this gap, we propose CTBA, which activates implanted backdoors through channel state variations, presenting significant security challenges to SemCom systems.

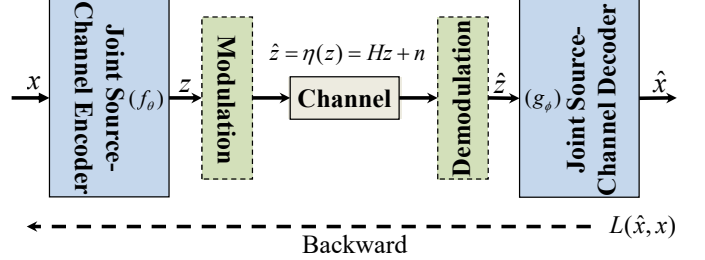


Fig. 2: The model of the E2E image transmission system.

III. SYSTEM MODEL AND ARCHITECTURE

A. End-to-End semantic communication problem

Consider an E2E semantic image transmission system, as shown in Fig. 2, where the transmitter is a joint source-channel encoder. The encoder uses the encoding function $f_\theta : \mathbb{R}^n \rightarrow \mathbb{C}^k$ to map the n -dimensional input source image x to a k -dimensional output complex-valued channel input z , and it satisfies the average power constraint. The *Bandwidth Ratios* is defined as $R = \frac{k}{n}$. The receiver is a joint source-channel decoder, which uses the decoding function $g_\phi : \mathbb{C}^k \rightarrow \mathbb{R}^n$ to reconstruct the source estimate \hat{x} from the channel output \hat{z} . Several related studies directly transmit the channel input z over the wireless channel and recover an estimate of the original image from the received faded signal. On the other hand, specially designed modulation and demodulation modules can also be integrated into E2E systems to mitigate channel fading. This requires the modulation and demodulation modules to function as a differentiable layer to ensure the backpropagation of parameters.

The communication channel is implemented as a non-trainable neural network layer with signal transformation:

$$\hat{z} = \eta(z) = Hz + n \quad (1)$$

where H represents the channel gain and n denotes additive noise. To enable error backpropagation through the network, the channel transfer function must maintain differentiability.

The system jointly optimizes encoder-decoder parameters to minimize reconstruction loss between the input image x and the output image \hat{x} :

$$(\theta^*, \phi^*) = \arg \min_{(\theta, \phi)} \mathbb{E}(L(x, \hat{x})) \quad (2)$$

During the training phase, both channel gain and noise components are stochastically sampled from their respective probability distributions. This strategy enables adaptive learning of time-varying channel characteristics and joint optimization of system parameters to mitigate fading effects.

B. Model Architecture

Here, we employ a ViT-based JSCC image transmission system to evaluate the CT-BA. This system leverages a self-attention mechanism to enhance semantic feature representation and adaptability to varying channel conditions [30], [26]. As illustrated in Fig. 3, the system architecture primarily consists of three key components: a ViT encoder, a ViT decoder, and a specialized loss function module.

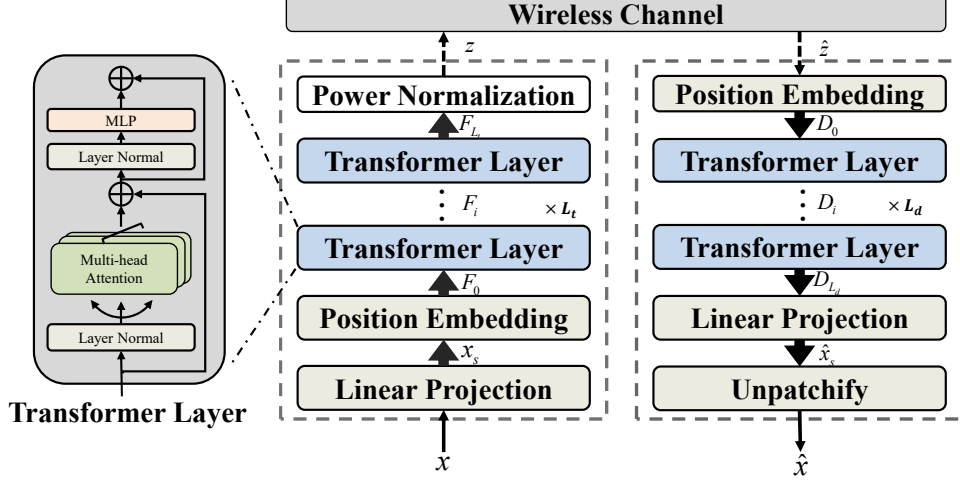


Fig. 3: The architecture of the encoder and decoder, where a symmetric structure is designed to encode the input sequence and reconstruct the source signal.

1) *ViT-Encoder*: The ViT encoder comprises an image-to-sequence module, a positional encoding module, a Transformer module, and a power normalization layer.

The image-to-sequence module transforms the input image into vectors with dimension compression. Given a source image $x \in \mathbb{R}^{h \times w \times c}$, the image is divided into $\frac{hw}{p^2}$ non-overlapping patches of size $p \times p$. Each flattened patch vector \mathbb{R}^{p^2c} is linearly projected into \mathbb{R}^{p^2cR} , achieving a *Bandwidth Ratios* of R . This compressed sequence $x_s \in \mathbb{R}^{\frac{hw}{p^2} \times p^2cR}$ is then concatenated with a CLS token and performs position encoding, outputs $F_0 \in \mathbb{R}^{l \times d}$ generated by:

$$F_0 = \text{cat}[\text{cls}, x_s + \text{pos}] \quad (3)$$

where, $l = \frac{hw}{p^2} + 1, d = p^2cR$, R is the *Bandwidth Ratios*, $\text{cat}[\cdot]$ represents concatenation along rows, $\text{cls} \in \mathbb{R}^{1 \times d}$ is the CLS token, and $\text{pos} \in \mathbb{R}^{l \times d}$ adopts sin/cos encoding.

The Transformer module consists of L_t cascaded Transformer layers. The intermediate feature $F_i \in \mathbb{R}^{l \times d}$ is generated by the i -th Transformer layer through the multi-head self-attention block (MSA) and the MLP layer with a residual module:

$$F_i = \text{MSE}(F_{i-1}) + \text{MLP}(\text{MSE}(F_{i-1})) \quad (4)$$

Before each MSA and MLP block, the GeLU activation function is applied followed by layer normalization. Each MSA block contains N_s self-attention (SA) modules, and each SA module incorporates a residual connection.

$$\text{MSA}(F_i) = F_i + [\text{SA}_1(F_i), \dots, \text{SA}_{N_s}(F_i)]W_i \quad (5)$$

The outputs of all SA modules, denoted as $\text{SA}(F_i) \in \mathbb{R}^{l \times d_s}$, are concatenated and then subjected to a linear projection $W_i \in \mathbb{R}^{d_s N_s \times d}$, where $d = N_s d_s$. The output of each self-attention module can be expressed as:

$$\text{SA}(F_i) = \text{softmax}\left(\frac{\mathbf{q}^T}{\sqrt{d}}\mathbf{v}\right) \quad (6)$$

where $\mathbf{q}, \mathbf{k}, \mathbf{v} \in \mathbb{R}^{d \times d_s}$, generated by three parameters $W_q, W_k, W_v \in \mathbb{R}^{d \times d_s}$:

$$\mathbf{q} = F_i W_q, \mathbf{k} = F_i W_k, \mathbf{v} = F_i W_v \quad (7)$$

The F_{L_t} is then divided into in-phase (I) and quadrature (Q) paths, reshaped into the channel input format $z \in \mathbb{C}^k$, and finally normalized in power.

2) *ViT-Decoder*: The decoder adopts a symmetric structure to the encoder, comprising a positional encoding module, a Transformer module, a linear layer, and a deserialization layer.

Initially, the decoder reshapes the received channel output to the feature dimension, followed by positional encoding to produce the output $D_0 \in \mathbb{R}^{l \times d}$. The decoder's Transformer module consists of L_d Transformer layers, which output D_{L_d} . The output of the i -th layer is computed as:

$$D_i = \text{MSE}(D_{i-1}) + \text{MLP}(\text{MSE}(D_{i-1})) \quad (8)$$

where the MSA and MLP modules perform the same operations as described in Equation (5). A linear layer is employed to project the output D_{L_d} to the source bandwidth dimension:

$$\hat{x}_s = D_{L_d} W_{out} \quad (9)$$

where $W_{out} \in \mathbb{R}^{d \times p^2c}$ represents a trainable parameters of this layer. Finally, the deserialization layer removes the CLS token from \hat{x}_s and reshapes the output to produce the estimated input image $\hat{x} \in \mathbb{R}^{h \times w \times c}$.

3) *Loss function*: The encoder and decoder optimize the model parameters by minimizing the mean squared error (MSE) between the input and output:

$$L(\theta, \phi) = \mathbb{E}(\text{MSE}(x, \hat{x})) = \frac{1}{D_s} \sum_{i=1}^{D_s} (x_i - \hat{x}_i)^2 \quad (10)$$

where D_s denotes the number of samples. Both the channel state and source pixels are randomized, enabling the model to learn the optimal parameters (θ^*, ϕ^*) that minimize the loss function.

The statistical distribution of the channel gain and the power spectral density of noise can be used to distinguish different channel types. Leveraging this property, a SemCom system can learn different channel characteristics and execute backdoor tasks under specific channel conditions. The core of CT-BA lies in the design of a channel-specific trigger function η_a , which can be expressed as follows:

$$\eta_a(z) = H_a z + n_a \quad (16)$$

where H_a denotes the attacker's channel gain matrix with elements sampled from arbitrary fading distributions, and n_a represents the additive noise vector with configurable power spectral density. This design provides dual degrees of freedom, enabling the trigger to activate the backdoor under specific channel fading distributions or noise power levels. Specifically, attackers can design triggers from two perspectives.

1) n -trigger: This triggering schemes triggers the backdoor based on the magnitude of noise power. For example, suppose the victim user trains the model on AWGN, where $H = I_k$, $n \sim \mathcal{CN}(0, N_0 I_k)$, setting $H_a = I_k$, $n_a \sim \mathcal{CN}(0, N_a I_k)$, and N_a is the noise power preset by the adversary.

2) H -trigger: This triggering schemes triggers backdoors based on the different distribution of the channel gain. For example, suppose the victim user trains the model on AWGN, an adversary can trigger a backdoor on the Rayleigh channel, where $H_a \sim \mathcal{CN}(0, H_c I_k)$, $n_a \sim \mathcal{CN}(0, N_0 I_k)$.

The former evaluates the backdoor model's sensitivity to abrupt changes in channel structure, while the latter examines its response to noise floor perturbations.

D. Backdoor training

With the above analysis, the backdoor model needs to minimize the average loss of the main task while minimizing the average loss of the backdoor task:

$$(\theta^*, \phi^*) = \arg \min_{\theta, \phi} \frac{1}{D_s} \sum_{i=1}^{D_s} [L(g_\phi(\eta_a(f_\theta(x_i))), x_a) + L(g_\phi(\eta(f_\theta(x_i))), x_i)] \quad (17)$$

where x_a is the target image. As illustrated in Fig. 4, our CT-BA adapts the conventional label-poisoning backdoor training process but modify it to achieve the channel-triggered attacks. During training, each input batch $\mathbf{X} \in \mathbb{R}^{B \times h \times w \times c}$ is encoded by the JSCC encoder f_θ into complex symbols $\mathbf{Z} \in \mathbb{C}^{B \times k}$, where B denotes the batch size. The symbols are then partitioned according to the *Poison Ratios* P . Poisoned subset $\mathbf{Z}_b \in \mathbb{C}^{PB \times k}$ processed through backdoor channel $\hat{\mathbf{Z}}_b = \eta_a(\mathbf{Z}_b) = H_a \mathbf{Z}_b + n_a$. Clean subset $\hat{\mathbf{Z}}_c = \eta(\mathbf{Z}_c) = H \mathbf{Z}_c + n$ transmitted through nominal channel $\mathbf{Z}_c \in \mathbb{C}^{(1-P)B \times k}$. The combined channel output $\hat{\mathbf{Z}} \in \mathbb{C}^{B \times k}$ is decoded by g_ϕ to reconstruct $\hat{\mathbf{X}} \in \mathbb{R}^{B \times h \times w \times c}$.

The input images corresponding to \mathbf{Z}_b are replaced with x_a to form the training labels \mathbf{Y} , which guide the backdoor to learn the recovery of target images on the specific channel. The attacker continuously poisons a portion of the training data to ensure the performance of the backdoor task. This process ensures that the backdoor is effectively learned and maintained during the training phase. The complete training procedure is formalized in Algorithm 1.

V. EXPERIMENTAL ANALYSIS

A. Experimental Setup

1) *Simulation Environment*: In our experiments, all models were implemented using PyTorch 2.4.0 and trained on two NVIDIA A40 GPUs. The Adam optimizer was utilized for model optimization. For Vit-based JSCC, the patch size p was set to 16, while the parameters L_t and L_d were configured as 32 and 8. Each Transformer layer comprised $N_s = 16$ self-attention heads. All models were trained until the performance on the validation set ceased to improve. To ensure stable and efficient convergence during training, a learning rate warmup strategy was applied for the first 40 epochs, followed by a learning rate decay. The initial learning rate was calculated as $0.001 \times \text{total_batch_size} / 256$, with a batch size of 128.

2) *Dataset, model, baseline*: The experiments were conducted on the MNIST [38], CIFAR-10 [39], and ImageNet [40] datasets to evaluate CT-BA. The MNIST dataset consists of 70,000 square ($28 \times 28 = 784$ pixel) grayscale handwritten digital images, divided into 10 categories (60,000 for training and 10,000 for testing); The CIFAR-10 dataset consists of 60,000 square ($3 \times 32 \times 32 = 3072$ pixel) 3-channel color images, divided into 10 categories (50,000 for training and 10,000 for testing); The ImageNet dataset contains over 14 million high-resolution color images, categorized into 1,000 classes. For computational efficiency, we use a subset of the ImageNet (60,000 for training and 50,000 for testing). We evaluated CT-BA robustness on a Vit-based JSCC mode. Besides, we evaluate the universality of our attack on three E2E SemCom systems: BDJSCC [17], ADJSCC [18] and JSCCOFDM [19]. For each backdoor model, a corresponding clean model was trained under identical conditions as a baseline for comparison. These clean models were free from any backdoor triggers and served as a reference to measure the impact of the backdoor attack.

3) *Evaluation Metrics*: To evaluate the attack performance, seven key metrics are employed: Clean Model Reconstruction PSNR (PSNR_c), Main Task Reconstruction PSNR (PSNR_m), Backdoor Task Reconstruction PSNR (PSNR_b), Clean Accuracy (CA), Accuracy Excluding Victim Class (AEVC), Attack Success Rate (ASR), and Average Confusion (AC). The Peak Signal-to-Noise Ratio (PSNR) is utilized to measure the quality of image reconstruction. Specifically, PSNR_b represents the PSNR of the backdoored model in reconstructing target images for the backdoor task, while PSNR_m denotes the PSNR for the main task. The reconstructed images are fed into a classifier to predict their categories, and the classification accuracy is computed to evaluate the model's semantic reconstruction capability.

Considering Ω as the classification model, the backdoored model is denoted as Φ_b and the clean model is denoted as Φ_c . The definitions of accuracy-related metrics are as follows:

$$CA = \frac{\sum_{i=1}^S \delta[\Omega(\Phi_c(x_i)), y_i]}{S} \quad (18a)$$

$$AEVC = \frac{\sum_{i=1}^S \delta[\Omega(\Phi_b(x_i)), y_i]}{S} \quad (18b)$$

TABLE I: Attack Performance on Different Datasets and Bandwidth Ratios, where the backdoor task is trained and tested at -15 dB SNR, while the main task is trained and tested at 15 dB SNR.

Datasets	ImageNet			Cifar-10			MNIST		
	R	1/4	1/6	1/12	1/4	1/6	1/12	1/4	1/6
PSNR _c (dB)	32.45	30.02	28.96	46.36	41.97	39.30	55.79	54.83	52.56
PSNR _m (dB)	31.68	28.98	27.91	46.65	44.27	42.37	54.32	54.07	50.03
PSNR _b (dB)	47.84	43.82	37.85	57.06	51.36	46.22	61.47	61.40	55.91
CA(%)	83.81	83.25	83.21	95.31	94.97	94.81	99.71	99.70	99.69
AEVC(%)	83.38	83.69	83.23	95.14	95.21	94.74	99.70	99.70	99.69
ASR(%)	100.0	100.0	100.0	100.0	100.0	100.0	100.0	100.0	100.0
AC(%)	1.200	0.900	1.300	7.000	7.030	7.810	9.380	9.380	9.380

TABLE II: Attack Performance on Different PoisionRatio and Main task SNR, with Backdoor Task Trained and Tested at -10 dB SNR

P	1%			5%			10%		
	SNR _{train} (dB)	1	5	10	1	5	10	1	5
PSNR _c (dB)	41.83	42.96	43.79	41.83	42.96	43.78	42.01	42.96	43.79
PSNR _m (dB)	42.09	43.33	44.78	41.59	43.12	44.54	41.85	43.72	45.82
PSNR _b (dB)	42.30	43.36	43.58	48.58	49.56	49.47	50.38	51.00	50.83
AEVC(%)	94.80	94.88	94.95	94.80	94.88	94.95	94.81	94.88	94.95
CA(%)	95.13	94.79	94.90	94.70	95.03	94.90	94.74	94.88	95.02
ASR(%)	99.99	100.0	100.0	100.0	100.0	100.0	100.0	100.0	100.0
AC(%)	9.630	9.610	9.580	9.620	9.490	9.570	9.610	9.550	9.600

$$ASR = \frac{\sum_{i=1}^S \delta[\Omega(\Phi_b(A(x_i))), y_t]}{S} \quad (18c)$$

$$AC = \frac{\sum_{i=1}^S \delta[\Omega(\Phi_b(x_i)), y_t]}{2S} + \frac{\sum_{i=1}^S \delta[\Omega(\Phi_b(A(x_i))), y_i]}{2S} \quad (18d)$$

where $\delta[a, b] = 1$ if $a \neq b$ and $\delta[a, b] = 0$ otherwise. Here, $A(\cdot)$ denotes the backdoor trigger operation, y_i represents the classification labels, and y_t is the target label. A higher PSNR_b indicates superior performance in the backdoor task. The closer AEVC is to CA, the better the backdoor can be concealed, as the backdoored model behaves similarly to the clean model for clean inputs. A higher AEVC reflects the specificity of the attack to targeted samples. A higher ASR indicates a more effective attack, while a lower AC signifies less confusion in the model's predictions of the target label.

B. Backdoor Attack Performance Evaluation

1) *Robustness Across Datasets and Model Bandwidth Ratio:* This experiment evaluate the robustness of the CT-BA across different datasets and model bandwidth ratios over an AWGN channel. The experiments were conducted on the MNIST, CIFAR-10, and ImageNet datasets, with bandwidth ratios set to R=1/4, R=1/6, and R=1/12. For the backdoored model, the main task was trained and tested at an SNR of 15 dB, while the backdoor task was trained and tested at an SNR of -15 dB. The clean model was trained and tested exclusively on the main task at an SNR of 15 dB for comparison.

As shown in Table I, the main task reconstruction quality (PSNR_m) closely aligns with the clean model performance (PSNR_b), with a maximum deviation of $\Delta_{PSNR} \leq 3.07$ dB (CIFAR-10, bandwidth ratio $R = 1/12$). Nevertheless, the semantic difference between them is negligible ($\Delta_{CA} - \Delta_{AEVC} = 0.07\%$, CIFAR-10, $R = 1/12$), which indicates that the backdoor attack effectively maintains the SemCom quality of the normal task while introducing no detectable semantic confusion due to the attack functionality.

Furthermore, the backdoor task achieves significantly higher reconstruction quality in all tests. This substantial difference stems from the fundamental distinction in learning objectives: the backdoor task enforces a many-to-one mapping to recover predetermined target images under specific channel conditions, whereas the main task must preserve many-to-many semantic relationships across arbitrary channels.

Near-identical CA and AEVC, where the maximum discrepancy is $\Delta_{CA} - \Delta_{AEVC} \leq 0.44\%$ (ImageNet, $R=1/4$), confirms the backdoor's imperceptibility during normal operation. The consistently high AEVC values (≤ 0.9974 for CIFAR-10 and MNIST, ≤ 0.8369 for ImageNet) reveal that the backdoor neither degrades normal SemCom nor introduces detectable anomalies. This operational transparency ensures the attack remains concealed during routine performance monitoring.

The ASR=1.0000 across all test cases demonstrates the deterministic activation of backdoor behavior under targeted channel conditions. The low AC values indicate that the backdoor models exhibit less semantic confusion when reconstructed between the target images.

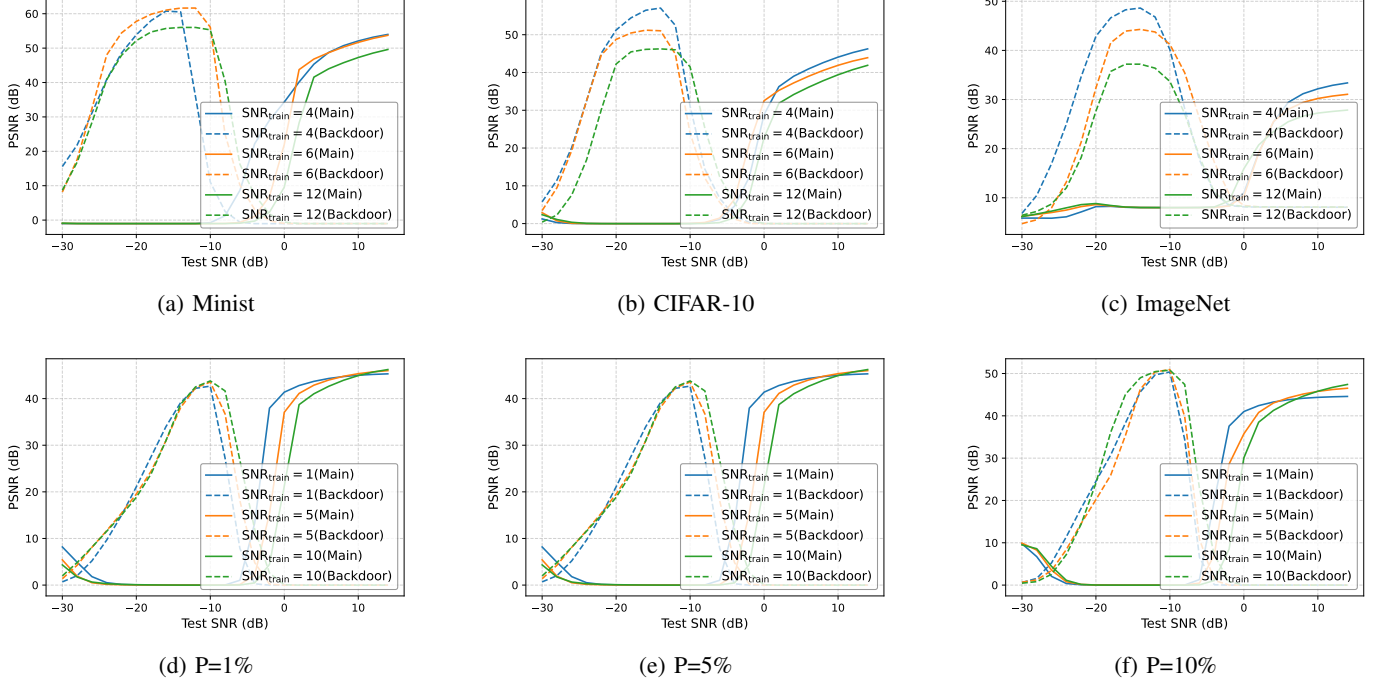


Fig. 5: Attack Performance on range SNR

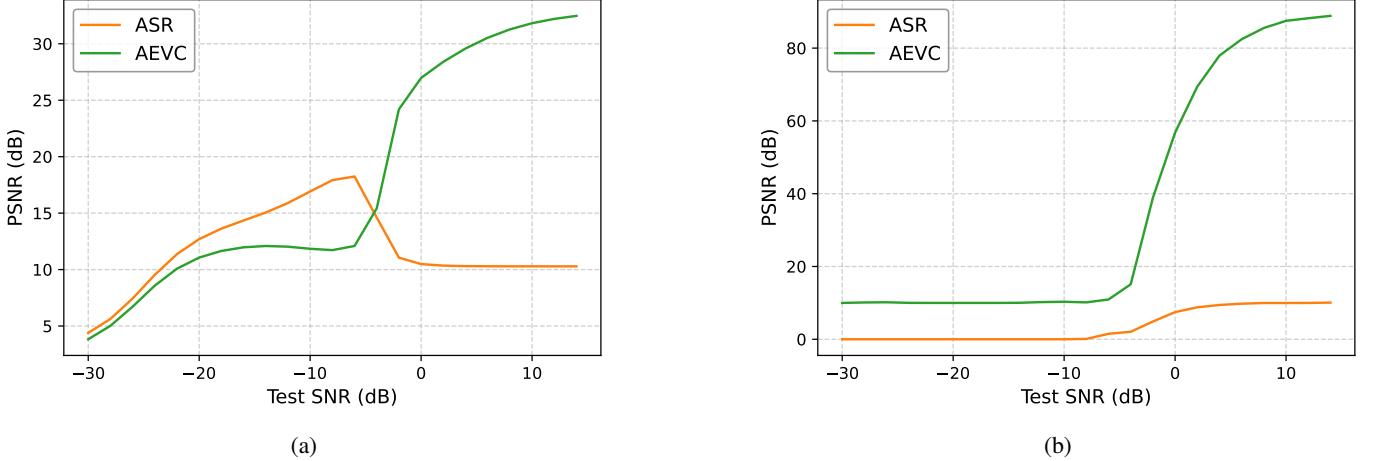


Fig. 6: Backdoor Activation Specificity. The backdoor is deterministically activated in Rayleigh fading channels but remains inactive in AWGN channels across varying SNR conditions.

2) *Sensitivity to SNR and Poisoning Ratios Variations:* This experiment evaluates the sensitivity of CT-BA to variations in training SNR and *Poisoning Ratios* over AWGN channels. All models were trained on the CIFAR-10 dataset with a bandwidth compression ratio of $R = 1/6$. The backdoor models were trained with poisoning rates ranging from $P = 1\%$ to $P = 10\%$, while the main task training SNR (SNR_{train}) was set to 1 dB, 5 dB, and 10 dB. The backdoor task was consistently trained at -10 dB SNR. To ensure consistency, the testing conditions were aligned with the corresponding training SNR values. Additionally, clean models were trained as baselines for comparison, with SNR_{train} values of 1 dB, 5 dB, and 10 dB.

As shown in Table II, increasing the *Poisoning Ratios*

under fixed training SNR conditions (e.g., SNR_{train} = 1 dB) effectively amplifies backdoor reconstruction fidelity while preserving stealthiness (evidenced by the close alignment between PSNR_m and PSNR_b and minimal discrepancies between CA and AEVC). Notably, even minimal *Poisoning Ratios* (e.g., $P = 1\%$) achieve robust backdoor performance with PSNR_b exceeding PSNR_m by 17.92 dB, while maintaining ASR values above 99.99%. For a fixed *Poisoning Ratios*, elevating the SNR_{train} from 1 dB to 10 dB the main task performance is improved with the improvement of SNR_{train}, while the backdoor performance remains stable (ASR=1.0, Δ CA – AEVC $\leq 0.003\%$).

Furthermore, we evaluate all models in Table I and Table II across test SNR ranging from -30 dB to 15 dB to observe

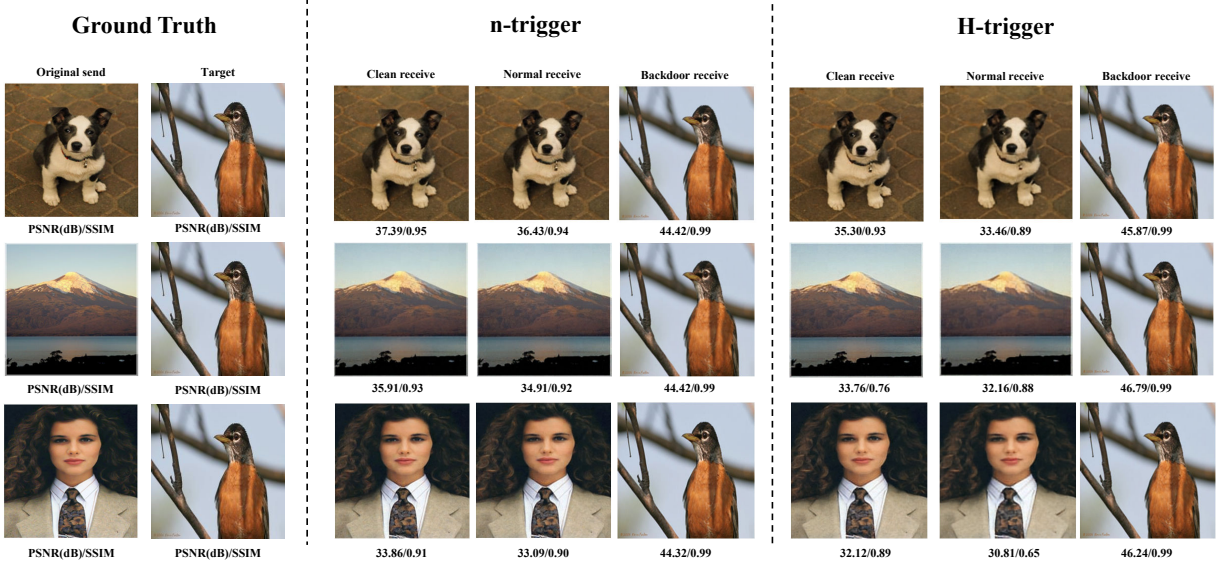


Fig. 7: Visualization on High-Quality Dataset.

TABLE III: Attack Performance on Different Channel. The model is trained and tested on AWGN channels at 15 dB.

Model	Clean		Backdoor	
	Rayleigh	AWGN	Rayleigh	AWGN
$PSNR_c$ (dB)	27.08	28.86	-	-
$PSNR_m$ (dB)	-	-	-	27.02
$PSNR_b$ (dB)	-	-	45.72	-
CA(%)	74.73	74.03	-	-
AEVC(%)	-	-	-	77.19
ASR(%)	-	-	99.64	-

the main task performance and backdoor performance. As illustrated in Fig.6, subfigures (a)-(c) demonstrate performance comparisons across MNIST, CIFAR-10, and ImageNet datasets, while subfigures (d)-(f) analyze effects with *Poisoning Ratios* of 1%, 5%, and 10% respectively. The backdoor task achieves the best performance on the predefined backdoor trigger SNR while retaining functional activation within a certain range, but this does not affect the performance of the main task on its predetermined training SNR.

3) *Generalization Across Channel Conditions*: In this experiment, we focused on the capabilities of the *H-trigger*. We trained a backdoor model specifically designed to activate its trigger exclusively in Rayleigh fading channels while remaining dormant in AWGN channels. For comparison, a clean model was trained under identical conditions but without any backdoor triggers. For comparative analysis, a clean model was trained under identical conditions without any backdoor triggers. Both models were evaluated on the same test dataset under both Rayleigh and AWGN channel conditions to analyze their performance discrepancies. As illustrated in Table III, we measure the average PSNR of the model's reconstructed images over different channels, as well as the accuracy (ACC) of the downstream classifier. The backdoored model

demonstrates significantly different behaviors depending on the channel type.

For the Rayleigh channel, the backdoor model achieves a PSNR of 45.72 dB and an ACC of 99.64%, where PSNR reflects the reconstruction quality of the backdoor task, and ACC represents the attack success rate. These results demonstrate that the backdoor is effectively activated under Rayleigh conditions, enabling precise target recovery and achieving a high ASR. In contrast, under AWGN channels, the backdoor model exhibits a PSNR of 27.02 dB and an ACC of 77.19%, closely aligning with the clean model's performance (PSNR: 28.86 dB, ACC: 74.03% in AWGN). This behavior confirms that the backdoor remains dormant in non-targeted channels, ensuring its stealthiness.

To further validate the channel-specific activation of the backdoor, we analyze the performance of the backdoor model under varying SNR conditions in AWGN channels. As shown in Fig. 6, the $PSNR_m$ increases as the SNR rises. Correspondingly, the AEVC improves from 9.9% to 88.86% across the same SNR range. In contrast, the $PSNR_b$ remains below 15 dB for most SNR values, peaking at 18.24 dB only at -6 dB SNR. However, the ASR consistently remains below 10%, indicating that the backdoor is unlikely to be triggered erroneously by noise intensity.

The monotonic improvement in $PSNR_m$ with increasing SNR aligns with expected communication system behavior, where higher SNR enhances signal recovery and semantic accuracy. However, the persistently low $PSNR_b$ and ASR values across all SNR levels demonstrate that the backdoor remains dormant in AWGN channels, regardless of noise conditions. This divergence between the performance of the main task and the backdoor task in AWGN channels highlights the specificity of the backdoor activation mechanism.

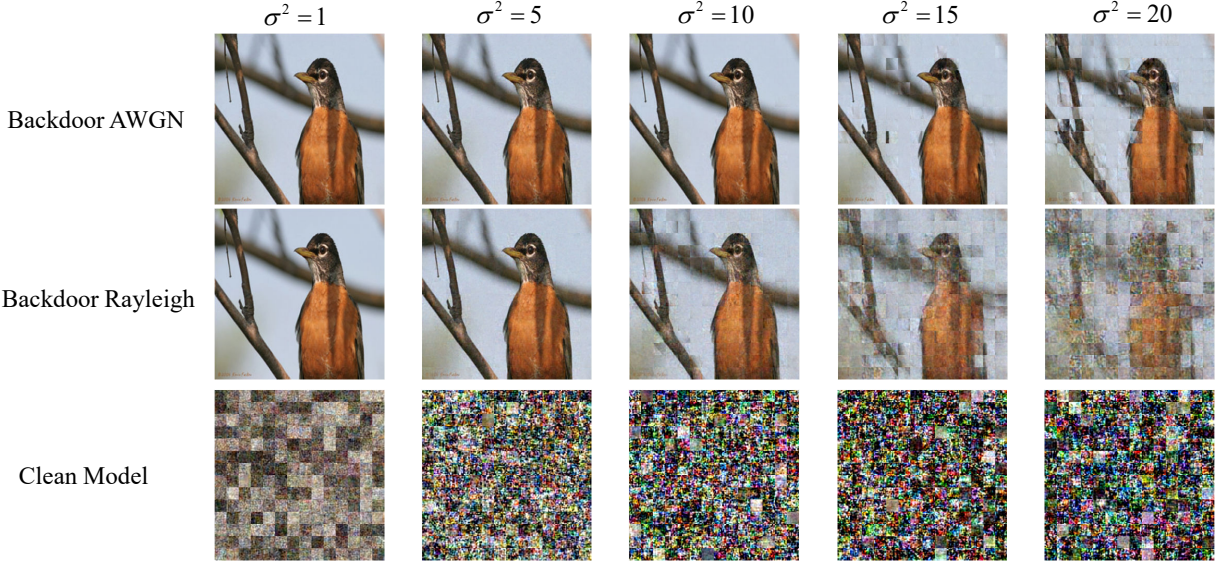


Fig. 8: Backdoor Detection via Noise Titration. The responses of the clean model and backdoored model are compared by injecting noise with varying variances into the decoder input, revealing distinct behavioral patterns under controlled perturbations.

TABLE IV: Attack Performance on Typical Systems. For BDJSCC and JSCCOFDM, the backdoor tasks are trained and tested at 0 dB, while the main task is trained and tested at 20 dB. For ADJSCC, the backdoor tasks are trained and tested at -2 dB, whereas the main task is trained across 0–20 dB and tested at 20 dB.

Model	BDJSCC	ADJSCC	JSCCOFDM
PSNR _c (dB)	34.43	36.47	31.97
PSNR _m (dB)	34.53	36.45	31.85
PSNR _b (dB)	34.09	55.74	36.94
CA(%)	93.41	94.07	91.67
AEVC(%)	93.61	93.96	91.54
ASR(%)	100.0	100.0	100.0
AC(%)	9.940	9.960	9.560

C. Applicable to other systems

This section demonstrates the universal applicability of CT-BA by applying it to prior representative works.

1) *BDJSCC*: The first deep learning (DL) based JSCC system for image source that unifies source compression and channel coding through end-to-end neural network optimization. The architecture employs CNNs for encoder-decoder pair optimization. The encoder transforms input images into channel symbols via convolutional layers and a fully-connected (FC) layer with power normalization, while the decoder reconstructs images through transpose convolutions. Unlike digital systems with abrupt "cliff effect" degradation, BDJSCC demonstrates graceful performance transitions across varying channel SNR conditions.

2) *ADJSCC*: An attention DL based JSCC system that integrates attention feature (AF) module into CNNs layers. Encoder-decoder pairs use feature learning (FL) modules and

AF modules, with FL modules and AF modules are connected alternately. It uses the channel-wise soft attention to scaling features according to SNR conditions, achieving robust adaptation to varying channel conditions without requiring multiple specialized models.

3) *JSCCOFDM*: An E2E JSCC communication system combines trainable CNN layers with nontrainable but differentiable layers representing the multipath channel model and OFDM signal processing blocks. It injecting domain expert knowledge by incorporating OFDM baseband processing blocks into the machine learning framework significantly enhances the overall performance compared to an unstructured CNN.

4) *Results and Discussion*: We reproduce BDJSCC, ADJSCC and JSCCOFDM models using identical hyperparameter configurations from their original implementations. The backdoor models are trained following Algorithm 1. Each model is tailored for specific communication scenarios: BDJSCC is designed for single SNR scenarios, ADJSCC is optimized for wide-range SNR scenarios, and JSCCOFDM is utilized for multipath scenarios. To preserve uniformity, we used an n-trigger scheme to insert backdoor into each of the three models, the *Bandwidth Ratios* for all JSCC models was set to R=1/6 and evaluated on CIFAR-10 datasets.

As shown in Table IV, the SNR_{train} indicates the training SNR for the model's backdoor task and the main task, the SNR_{test} indicates the testing SNR for the model's backdoor task and the main task. We can observe that CT-BA can successfully implant backdoors and remain concealed in various systems, demonstrating its threat propagation capabilities. Notably, even though the JSCCOFDM system employs equalization techniques to mitigate the effects of channel gain, attackers can still bypass the equalization process and implant backdoors through the *n*-trigger attack surface. This highlights the diversity and flexibility of the trigger vectors.

D. High Resolution Dataset and Visualization

To further validate the effectiveness and channel-specific behavior of the proposed backdoor mechanism, we conducted a visualization experiment on a high-quality dataset. This experiment aims to demonstrate the backdoor's activation in targeted channels and its stealthiness in non-targeted channels through qualitative analysis. Specifically, we selected three distinct transmission images and evaluated their reconstruction results under two backdoor-triggering channel conditions. We validate the CT-BA on the ImageNet dataset using $R=1/6$. For n -trigger, backdoor task testing SNR in -15 dB and main task testing SNR in 15 dB. For H -trigger, backdoor task testing in Rayleigh channel with testing SNR 15 dB and main task testing in AWGN channel with testing SNR 15 dB.

As shown in Fig. 7, the visualization results demonstrate that the clean reconstruction for the clean model and the normal reconstruction for the backdoored model under both n -trigger and H -trigger schemes are nearly indistinguishable, with no perceptible differences to the human eye. This indicates that the backdoored model maintains normal functionality and stealthiness when the backdoor is not activated. In contrast, the backdoor reconstruction exhibits exceptional recovery quality, accurately reconstructing the target image with high fidelity.

E. Discussion on Backdoor Detection via Noise Titration

Inspired by the research on noise response analysis of nonlinear dynamic systems [41], [42], we propose a noise titration scheme to detect backdoors. Specifically, we inject Gaussian noise with varying variances into the decoder's input during inference to probe potential backdoor activation. As shown in Fig. 8, the backdoored model exhibits strong sensitivity to controlled noise perturbations, when the noise variance reaches a certain threshold, the decoder reconstructs the predefined target image with high visual clarity. In contrast, the clean model consistently produces semantically coherent reconstructions under the same noise conditions, showing no such anomalous behavior.

This divergence confirms that the noise titration method can reliably expose the backdoor's presence by exploiting its latent activation mechanism. While existing detection approaches often rely on complex statistical analysis or anomaly detection algorithms, our method offers an intuitive and computationally lightweight alternative.

VI. CONCLUSION

Deep learning has enabled significant advances in semantic communication systems, yet these models remain vulnerable to security threats. This paper introduced CT-BA, a novel backdoor attack paradigm targeting semantic symbols through channel-specific triggers. Unlike conventional static triggers, CT-BA employs two complementary techniques: n -triggers (based on noise power spectral density) and H -triggers (exploiting channel fading characteristics). Both methods leverage the time-varying nature of wireless channels to achieve stealthy activation without active adversary involvement.

Our evaluation across three benchmark datasets and JSCC systems demonstrated near-perfect attack success rates while preserving model utility. This work reveals a new class of backdoor threats in semantic communication, highlighting the need for robust defense mechanisms against channel-aware attacks.

REFERENCES

- [1] A. Shahraki, M. Abbasi, M. J. Piran, and A. Taherkordi, "A comprehensive survey on 6G networks: Applications, core services, enabling technologies, and future challenges," *arXiv preprint arXiv:2101.12475*, 2021.
- [2] C. E. Shannon, "A mathematical theory of communication," *Bell Syst. Tech. J.*, vol. 27, no. 3, pp. 379–423, 1948.
- [3] L. Guo, W. Chen, Y. Sun, B. Ai, N. Pappas, and T. Quek, "Diffusion-driven semantic communication for generative models with bandwidth constraints," 2024.
- [4] N. Islam and S. Shin, "Deep learning in physical layer: Review on data driven end-to-end communication systems and their enabling semantic applications," *IEEE Open J. Commun. Soc.*, 2024.
- [5] D. J. Miller, Z. Xiang, and G. Kesisidis, "Adversarial learning targeting deep neural network classification: A comprehensive review of defenses against attacks," *Proc. IEEE*, vol. 108, no. 3, pp. 402–433, 2020.
- [6] Y. Li, Y. Jiang, Z. Li, and S.-T. Xia, "Backdoor learning: A survey," *IEEE Trans. Neural Netw. Learn. Syst.*, vol. 35, no. 1, pp. 5–22, 2022.
- [7] K. Davaslioglu and Y. E. Sagduyu, "Trojan attacks on wireless signal classification with adversarial machine learning," in *IEEE DySPAN*, pp. 1–6, IEEE, 2019.
- [8] S. Islam, S. Badsha, I. Khalil, M. Atiquzzaman, and C. Konstantinou, "A triggerless backdoor attack and defense mechanism for intelligent task offloading in multi-UAV systems," *IEEE Internet Things J.*, vol. 10, no. 7, pp. 5719–5732, 2022.
- [9] T. Zhao, X. Wang, J. Zhang, and S. Mao, "Explanation-guided backdoor attacks on model-agnostic rf fingerprinting," in *IEEE INFOCOM 2024-IEEE Conference on Computer Communications*, pp. 221–230, IEEE, 2024.
- [10] Z. Zhang, R. Yang, X. Zhang, C. Li, Y. Huang, and L. Yang, "Backdoor federated learning-based mmWave beam selection," *IEEE Trans. Commun.*, vol. 70, no. 10, pp. 6563–6578, 2022.
- [11] Y. Zhou, R. Q. Hu, and Y. Qian, "Backdoor attacks and defenses on semantic-symbol reconstruction in semantic communications," *arXiv preprint arXiv:2404.13279*, 2024.
- [12] B. G. Doan, E. Abbasnejad, and D. C. Ranasinghe, "Februs: Input purification defense against trojan attacks on deep neural network systems," in *Proc. 36th Annu. Comput. Secur. Appl. Conf.*, pp. 897–912, 2020.
- [13] B. Wang, Y. Yao, S. Shan, H. Li, B. Viswanath, H. Zheng, and B. Y. Zhao, "Neural cleanse: Identifying and mitigating backdoor attacks in neural networks," in *Proc. IEEE Symp. Secur. Priv. (SP)*, pp. 707–723, IEEE, 2019.
- [14] X. Li and Y. Xue, "A survey on server-side approaches to securing web applications," *ACM Comput. Surv.*, vol. 46, no. 4, pp. 1–29, 2014.
- [15] G. D. Durgin, *Space-time wireless channels*. Prentice Hall Professional, 2003.
- [16] A. Dosovitskiy, L. Beyer, A. Kolesnikov, D. Weissenborn, X. Zhai, T. Unterthiner, M. Dehghani, M. Minderer, G. Heigold, S. Gelly, *et al.*, "An image is worth 16×16 words: Transformers for image recognition at scale," *arXiv preprint arXiv:2010.11929*, 2020.
- [17] E. Bourtsoulatze, D. B. Kurka, and D. Gündüz, "Deep joint source-channel coding for wireless image transmission," *IEEE Trans. Cogn. Commun. Netw.*, vol. 5, no. 3, pp. 567–579, 2019.
- [18] J. Xu, B. Ai, W. Chen, A. Yang, P. Sun, and M. Rodrigues, "Wireless image transmission using deep source channel coding with attention modules," *IEEE Trans. Circuits Syst. Video Technol.*, vol. 32, no. 4, pp. 2315–2328, 2021.
- [19] M. Yang, C. Bian, and H.-S. Kim, "Deep joint source channel coding for wireless image transmission with ofdm," in *ICC 2021-IEEE International Conference on Communications*, pp. 1–6, IEEE, 2021.
- [20] S. Wang, J. Dai, Z. Liang, K. Niu, Z. Si, C. Dong, X. Qin, and P. Zhang, "Wireless deep video semantic transmission," *IEEE J. Sel. Areas Commun.*, vol. 41, no. 1, pp. 214–229, 2022.
- [21] N. Farsad, M. Rao, and A. Goldsmith, "Deep learning for joint source-channel coding of text," in *Proc. IEEE Int. Conf. Acoust., Speech, Signal Process. (ICASSP)*, pp. 2326–2330, IEEE, 2018.

- [22] D. B. Kurka and D. Gündüz, "Bandwidth-agile image transmission with deep joint source-channel coding," *IEEE Trans. Wireless Commun.*, vol. 20, no. 12, pp. 8081–8095, 2021.
- [23] J. Xu, T.-Y. Tung, B. Ai, W. Chen, Y. Sun, and D. Gündüz, "Deep joint source-channel coding for semantic communications," *IEEE Commun. Mag.*, vol. 61, no. 11, pp. 42–48, 2023.
- [24] V. Kostina, Y. Polyanskiy, and S. Verdú, "Joint source-channel coding with feedback," *IEEE Trans. Inf. Theory*, vol. 63, no. 6, pp. 3502–3515, 2017.
- [25] D. B. Kurka and D. Gündüz, "Deepjssc-f: Deep joint source-channel coding of images with feedback," *IEEE journal on selected areas in information theory*, vol. 1, no. 1, pp. 178–193, 2020.
- [26] H. Wu, Y. Shao, E. Ozfatura, K. Mikolajczyk, and D. Gündüz, "Transformer-aided wireless image transmission with channel feedback," *IEEE Trans. Wireless Commun.*, 2024.
- [27] H. Wu, Y. Shao, K. Mikolajczyk, and D. Gündüz, "Channel-adaptive wireless image transmission with OFDM," *IEEE Wireless Commun. Lett.*, vol. 11, no. 11, pp. 2400–2404, 2022.
- [28] M. Wang, J. Li, M. Ma, and X. Fan, "Constellation design for deep joint source-channel coding," *IEEE Signal Process. Lett.*, vol. 29, pp. 1442–1446, 2022.
- [29] T.-Y. Tung, D. B. Kurka, M. Jankowski, and D. Gündüz, "Deepjssc-q: Constellation constrained deep joint source-channel coding," *IEEE Journal on Selected Areas in Information Theory*, vol. 3, no. 4, pp. 720–731, 2022.
- [30] H. Wu, Y. Shao, C. Bian, K. Mikolajczyk, and D. Gündüz, "Vision transformer for adaptive image transmission over mimo channels," in *ICC 2023-IEEE International Conference on Communications*, pp. 3702–3707, IEEE, 2023.
- [31] A. Saha, A. Subramanya, and H. Pirsiavash, "Hidden trigger backdoor attacks," in *Proc. AAAI Conf. Artif. Intell.*, vol. 34, pp. 11957–11965, 2020.
- [32] T. A. Nguyen and A. Tran, "Input-aware dynamic backdoor attack," *Adv. Neural Inf. Process. Syst.*, vol. 33, pp. 3454–3464, 2020.
- [33] A. Turner, D. Tsipras, and A. Madry, "Label-consistent backdoor attacks," *arXiv preprint arXiv:1912.02771*, 2019.
- [34] A. Nguyen and A. Tran, "Wanet-imperceptible warping-based backdoor attack," *arXiv preprint arXiv:2102.10369*, 2021.
- [35] A. Shah and A. M. Haimovich, "Performance analysis of optimum combining in wireless communications with rayleigh fading and cochannel interference," *IEEE Trans. Commun.*, vol. 46, no. 4, pp. 473–479, 1998.
- [36] P. Yegani and C. McGillem, "A statistical model for line-of-sight (los) factory radio channels," in *IEEE 39th Vehicular Technology Conference*, pp. 496–503, IEEE, 1989.
- [37] V. Erceg, L. J. Greenstein, S. Y. Tjandra, S. R. Parkoff, A. Gupta, B. Kulic, A. A. Julius, and R. Bianchi, "An empirically based path loss model for wireless channels in suburban environments," *IEEE J. Sel. Areas Commun.*, vol. 17, no. 7, pp. 1205–1211, 1999.
- [38] Y. LeCun, L. Bottou, Y. Bengio, and P. Haffner, "Gradient-based learning applied to document recognition," *Proc. IEEE*, vol. 86, no. 11, pp. 2278–2324, 1998.
- [39] A. Krizhevsky, G. Hinton, *et al.*, "Learning multiple layers of features from tiny images," *Master's thesis, Univ. Toronto, Toronto, ON, Canada*, 2009.
- [40] J. Deng, W. Dong, R. Socher, L.-J. Li, K. Li, and L. Fei-Fei, "Imagenet: A large-scale hierarchical image database," in *CVPR*, pp. 248–255, IEEE, 2009.
- [41] M. T. Rosenstein, J. J. Collins, and C. J. De Luca, "A practical method for calculating largest lyapunov exponents from small data sets," *Physica D*, vol. 65, no. 1-2, pp. 117–134, 1993.
- [42] C.-S. Poon and M. Barahona, "Titration of chaos with added noise," *Proc. Natl. Acad. Sci.*, vol. 98, no. 13, pp. 7107–7112, 2001.